

## MIT Open Access Articles

*Catalytically mediated epitaxy of 3D  
semiconductors on van der Waals substrates*

The MIT Faculty has made this article openly available. **Please share**  
how this access benefits you. Your story matters.

**Citation:** Periwal, Priyanka et al. "Catalytically mediated epitaxy of 3D semiconductors on van der Waals substrates." *Applied Physics Reviews*, 7, 3 (July 2020): 031402 © 2020 The Author(s)

**As Published:** 10.1063/5.0006300

**Publisher:** AIP Publishing

**Persistent URL:** <https://hdl.handle.net/1721.1/127768>

**Version:** Final published version: final published article, as it appeared in a journal, conference proceedings, or other formally published context

**Terms of use:** Creative Commons Attribution 4.0 International license









# Catalytically mediated epitaxy of 3D semiconductors on van der Waals substrates


F


Cite as: Appl. Phys. Rev. **7**, 031402 (2020); <https://doi.org/10.1063/5.0006300>

Submitted: 03 March 2020 . Accepted: 11 June 2020 . Published Online: 16 July 2020

Priyanka Periwal, Joachim Dahl Thomsen , Kate Reidy , Georgios Varnavides , Dmitri N. Zakharov , Lynne Cignac, Mark C. Reuter, Timothy J. Booth , Stephan Hofmann , and Frances M. Ross 

## COLLECTIONS

 This paper was selected as Featured

 This paper was selected as Scilight



View Online



Export Citation



CrossMark

## ARTICLES YOU MAY BE INTERESTED IN

[An intermediate catalytic crystal helps semiconductors grow epitaxially on 2D substrates](#)  
Scilight **2020**, 291109 (2020); <https://doi.org/10.1063/10.0001636>

[A monolithic artificial iconic memory based on highly stable perovskite-metal multilayers](#)  
Applied Physics Reviews **7**, 031401 (2020); <https://doi.org/10.1063/5.0009713>

[Photonic tensor cores for machine learning](#)  
Applied Physics Reviews **7**, 031404 (2020); <https://doi.org/10.1063/5.0001942>



AVS Quantum Science

SPECIAL ISSUE:  
Quantum Sensing and Metrology

SUBMIT TODAY!



# Catalytically mediated epitaxy of 3D semiconductors on van der Waals substrates

Cite as: Appl. Phys. Rev. **7**, 031402 (2020); doi: [10.1063/5.0006300](https://doi.org/10.1063/5.0006300)

Submitted: 3 March 2020 · Accepted: 11 June 2020 ·

Published Online: 16 July 2020



View Online



Export Citation



CrossMark

Priyanka Periwal,<sup>1,2</sup> Joachim Dahl Thomsen,<sup>3</sup> Kate Reidy,<sup>4</sup> Georgios Varnavides,<sup>4,5</sup> Dmitri N. Zakharov,<sup>6</sup> Lynne Gignac,<sup>2</sup> Mark C. Reuter,<sup>2</sup> Timothy J. Booth,<sup>3</sup> Stephan Hofmann,<sup>1,a)</sup> and Frances M. Ross<sup>2,4,a)</sup>

## AFFILIATIONS

<sup>1</sup>Department of Electrical Engineering, University of Cambridge, Cambridge CB3 0FA, United Kingdom

<sup>2</sup>IBM T. J. Watson Research Center, Yorktown Heights, New York 10598, USA

<sup>3</sup>Center for Nanostructured Graphene, Department of Physics, Technical University of Denmark, DK-2800 Kongens Lyngby, Denmark

<sup>4</sup>Department of Materials Science and Engineering, Massachusetts Institute of Technology, Cambridge, Massachusetts 02139, USA

<sup>5</sup>School of Engineering and Applied Sciences, Harvard University, Cambridge, Massachusetts, 02138, USA

<sup>6</sup>Center for Functional Nanomaterials, Brookhaven National Laboratory, Upton, New York 11973, USA

<sup>a)</sup>Authors to whom correspondence should be addressed: [fmross@mit.edu](mailto:fmross@mit.edu) and [sh315@cam.ac.uk](mailto:sh315@cam.ac.uk)

## ABSTRACT

The formation of well-controlled interfaces between materials of different structure and bonding is a key requirement when developing new devices and functionalities. Of particular importance are epitaxial or low defect density interfaces between two-dimensional materials and three-dimensional semiconductors or metals, where an interfacial structure influences electrical conductivity in field effect and optoelectronic devices, charge transfer for spintronics and catalysis, and proximity-induced superconductivity. Epitaxy and hence well-defined interfacial structure has been demonstrated for several metals on van der Waals-bonded substrates. Semiconductor epitaxy on such substrates has been harder to control, for example during chemical vapor deposition of Si and Ge on graphene. Here, we demonstrate a catalytically mediated heteroepitaxy approach to achieve epitaxial growth of three-dimensional semiconductors such as Ge and Si on van der Waals-bonded materials such as graphene and hexagonal boron nitride. Epitaxy is “transferred” from the substrate to semiconductor nanocrystals via solid metal nanocrystals that readily align on the substrate and catalyze the formation of aligned nuclei of the semiconductor. *In situ* transmission electron microscopy allows us to elucidate the reaction pathway for this process and to show that solid metal nanocrystals can catalyze semiconductor growth at a significantly lower temperature than direct chemical vapor deposition or deposition mediated by liquid catalyst droplets. We discuss Ge and Si growth as a model system to explore the details of such hetero-interfacing and its applicability to a broader range of materials.

© 2020 Author(s). All article content, except where otherwise noted, is licensed under a Creative Commons Attribution (CC BY) license (<http://creativecommons.org/licenses/by/4.0/>). <https://doi.org/10.1063/5.0006300>

## I. INTRODUCTION

To fully exploit the potential of the ever-increasing portfolio of two-dimensional (2D) materials<sup>1–3</sup> and three-dimensional (3D) self-assembled nanostructures,<sup>4,5</sup> the diverse components must be brought together in a well-controlled and reliable fashion. Of particular importance are epitaxial or low defect density interfaces between 2D materials and 3D semiconductors or metals,<sup>6–8</sup> as highlighted by recent literature ranging from improved electrical contacts for field effect and optoelectronic devices to charge transfer for spintronics and catalysis as well as proximity-induced superconductivity.<sup>7,9–16</sup> However, significant challenges are presented by the dissimilar chemical bonding and structure across interfaces between 3D and van der Waals-bonded

materials.<sup>6–8</sup> In several metal/van der Waals substrate combinations, such as Au on MoS<sub>2</sub>, epitaxial alignment and therefore highly ordered interfaces between the materials are well established.<sup>17–21</sup> But epitaxy of semiconductor nanostructures on van der Waals-bonded materials has been more challenging, for example during chemical vapor deposition of Si and Ge on graphene.<sup>22,23</sup> Here we introduce a catalytically mediated approach to achieve heteroepitaxial growth of 3D semiconductors on van der Waals materials. We focus on a model system, Ge on graphene or hexagonal boron nitride (hBN), and describe a strategy that combines the benefits of van der Waals epitaxy<sup>2</sup> and catalytic growth of nanostructures.<sup>4</sup> Under circumstances where the semiconductor (Ge) does not grow with good alignment to the substrate, we

show that alignment can be improved using solid catalytic nanocrystals (Au) that are themselves crystallographically aligned with the substrate. Epitaxy is thereby “transferred” from the van der Waals substrate via the solid catalyst to the semiconductor. We use a combination of *in situ* and post-growth transmission electron microscopy (TEM) to establish the relationship between the materials, explore the reaction pathways, and optimize the catalyst and growth conditions. We will show that this growth strategy can be extended to Si by growing Si nanocrystals epitaxially on graphene and hBN using solid catalysts composed of Au + Ag. This suggests that a broader range of group IV alloys and, potentially, heterostructures might be addressed with an appropriate choice of the catalyst material.

As well as enhancing epitaxial alignment, we find another advantage that the solid catalysts provide for Si and Ge epitaxy: the growth process takes place at lower temperatures compared to either conventional chemical vapor deposition (CVD) or growth from liquid catalyst droplets. This can, in principle, enable epitaxy of Si and Ge on, for example, temperature-sensitive substrates coated with graphene. Finally, we discuss how the growth strategy may apply to III-V semiconductor nanostructures. As an alternative to remote epitaxy,<sup>2</sup> catalytic growth of III-V nanostructures on van der Waals-bonded materials<sup>25,26</sup> can achieve epitaxial alignment even using liquid droplets, and solid catalysts may provide additional advantages.

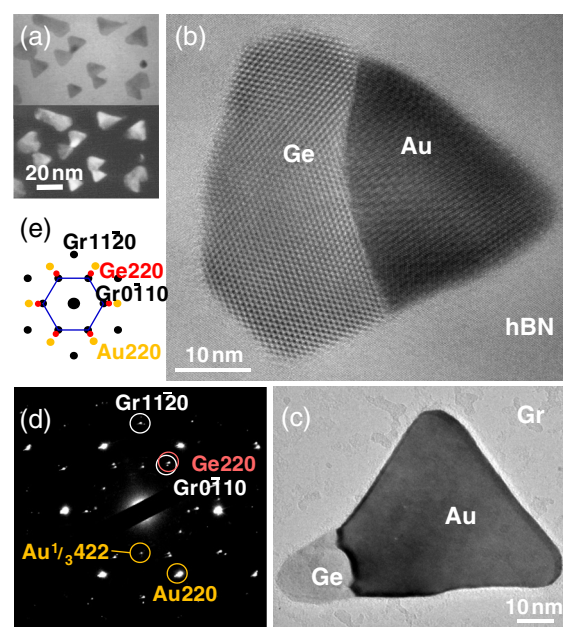
## II. EPITAXIAL Ge ON VAN DER WAALS SUBSTRATES

Figure 1 illustrates epitaxy of Ge on graphene and hBN using crystalline Au as the catalyst. Both *in situ* and post-growth imaging help to clarify the structures formed at each stage of the process.

The experiment starts with a substrate made up of a suspended membrane of trilayer graphene [Figs. 1(a) and 1(c)], or a much thicker (30 ML) hBN crystal with a thickness of 10 nm [Fig. 1(b)]. These layers are transferred using cellulose acetate butyrate (CAB) as a polymer handle,<sup>27</sup> and placed on a silicon nitride support patterned with holes, itself supported on Si. Details of the transfer procedure and sample geometry are provided in Sec. VI and in Fig. S1. This composite substrate is loaded into a custom TEM that has an ultra-high vacuum (UHV) sample environment and is connected to UHV chambers that have capabilities for thermal evaporation of metals and flow of CVD precursor gases (see Sec. VI). The sample is then cleaned by heating in UHV at 450 °C for several hours. This particular combination of polymer and heat treatment has been shown<sup>28,29</sup> to result in the near-complete removal of polymeric residues and carbon. Subsequently, we deposit typically 0.2 nm Au. The sample is then moved to the UHV-TEM column where the Au coverage, island shape, and epitaxial relationship with the underlying 2D material are measured.

Figure 1(a) shows that triangular, epitaxial Au nanocrystals have formed with the orientation relation shown in Fig. 1(e). This morphology has previously been reported for Au on graphite.<sup>30,31</sup> Post-growth analysis (Fig. S2) confirms that the Au islands are typically flat plates with an aspect ratio (height/edge length) of  $\sim 0.1$ . Figure S3 shows that the annealing treatment described above is necessary to achieve the quality of the epitaxy shown in Fig. 1, and that it is also necessary to avoid exposure of the 2D material to the imaging beam before Au deposition.

On heating the as-prepared sample to 170–200 °C and exposure to digermane gas ( $\text{Ge}_2\text{H}_6$ ), Ge crystals (diamond cubic, DC) selectively nucleate at the solid Au nanocrystals, as shown in Figs. 1(b) and 1(c).



**FIG. 1.** Transferred epitaxy of Ge on graphene and hBN via a solid catalyst. (a) Bright and dark field Au{220} image pair, upper and lower, respectively, recorded in the UHV-TEM directly after evaporation of 0.2 nm Au onto a graphene trilayer. (b, c) Post-growth images of Au islands with Ge grown at 190 °C using  $2 \times 10^{-5}$  Torr digermane. In (b) the substrate is 10 nm thick hBN and in (c) it is three-layer graphene. (d) Diffraction pattern obtained from the island in (c), showing the proximity of Ge and Gr spots. Additional  $\frac{1}{3}\langle 422 \rangle$  spots from Au are also visible. (e) Schematic diffraction pattern showing the Ge, graphene, and bulk Au spots.

This vapor-solid-solid (VSS) growth mechanism is consistent with previous observations (on conventional substrates) of catalytic nucleation and growth of Ge at low temperatures.<sup>32–34</sup> We find a similar outcome whether we use graphene [Fig. 1(c)] or hBN [Fig. 1(b)] and on various substrate thicknesses [10 nm in Fig. 1(b), 1 nm in Fig. 1(c)]. After nucleation, the Ge crystals continue to grow and the Au slowly deforms, as shown in Figs. 1(b) and 2(a) and discussed below.

The epitaxial relationship of face-centered cubic (FCC) Au and DC Ge on the hexagonal van der Waals-bonded substrate can be rationalized with simple considerations of the symmetry and nearest neighbor distances of each material. For FCC Au, symmetry suggests that  $\langle 111 \rangle$  should be out of plane; Au  $\langle 110 \rangle$  could then be parallel to either the  $\langle 0\bar{1}10 \rangle$  or  $\langle 11\bar{2}0 \rangle$  directions of the 2D material. The former case is evident from the diffraction pattern in Fig. 1(d) since the Au (220) and graphene  $\langle 0\bar{1}10 \rangle$  spots are in alignment. This orientation relation is expected from prior studies of epitaxial Au on the basal plane of graphite.<sup>30</sup> The consequence of this orientation relation is shown in Fig. 3. In the structure in Fig. 3(a), the atoms are in close registry because the nearest neighbor distances are 0.142 nm for graphene, 0.144 nm for hBN, and almost exactly twice this value, 0.288 nm, for Au.

When Ge is added, the nanocrystals predominantly show an orientation with cube axes parallel to Au, as seen from diffraction and dark field imaging [Figs. 1, 3, and S5]. The nearest neighbor distance for Ge is 0.244 nm, so the experimentally determined orientation leads to a structure in which three Ge spacings are in registry with 5 carbon

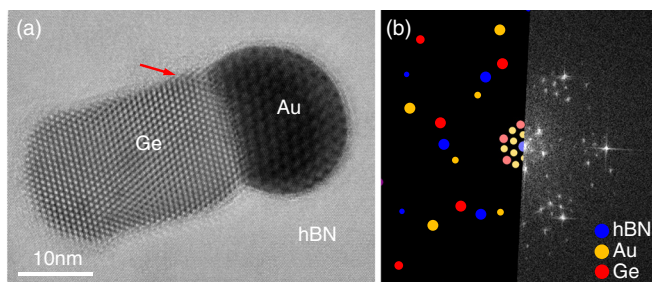


**FIG. 2.** Alignment of Au and Ge lattices. (a) An Au island and its nucleated Ge on 10-nm thick hBN imaged after growth at 190 °C with  $2 \times 10^{-5}$  Torr digermene. The strong moiré contrast, with period 0.91 nm in the Ge and 1.85 nm in the Au, arises from the superposition of the hBN lattice with the Au and Ge lattices. The change in moiré contrast in the Ge at the arrow may indicate a defect in the Ge. (b) (Right) Fast Fourier transform (FFT) of a region of the image containing all three lattices. (Left) Simulated diffraction pattern for an orientation relation between the three lattices. The calculated moiré periods are shown as the lighter central spots. (Similar spots are expected around each diffracted spot but not shown.) To match the experimental moiré contrast, the Au and Ge(220) directions are both 14° from the hBN  $\langle 01\bar{1}0 \rangle$  directions.

spacings along the  $\langle 220 \rangle$  direction with only 3% mismatch [1.6% for hBN, Fig. 3(a)].

During the nucleation and growth of the Ge nanocrystals, we propose that the van der Waals substrate does not determine the nanocrystal orientation through direct contact; instead, each Ge inherits its orientation from its Au catalyst rather than directly from the substrate as in conventional epitaxy. We deduce this “transfer of epitaxy” by examining nanocrystals that are misaligned with the substrate. Figure 2(a) shows an Au catalyst that has nucleated a large Ge crystal. Moiré patterns are visible in both Ge and Au due to the superposition in the beam direction of each lattice and the thick hBN substrate. Analysis of the period and angle of the moiré contrast visible in the Au [Fig. 2(b), see Sec. VI] shows that the Au lattice is rotated by

14° from the arrangement described above and in Fig. 1(e). Independent analysis of the moiré contrast in the Ge yields the same rotation. We conclude that in this case the Au and Ge have a cube-on-cube orientation relationship, while both are misoriented with respect to the substrate. With occasional exceptions [such as the arrowed region in Fig. 2(a)], neither Au nor Ge moiré patterns in the nanocrystals analyzed show evidence of crystal defects, and no strain needs to be included to match the observed patterns.

To quantify the growth kinetics of individual Ge nanocrystals, we show in Figs. 4(a) and 4(b) sequential images recorded during growth. As might be expected, each Au triangle typically nucleates a single Ge crystal at a vertex [Fig. 4(d)], although edge or re-entrant nucleation sites are possible [Fig. 4(c) and S4]. In Movie M1 and Fig. 4(a), Ge grows more slowly at two triangular Au islands than at a nearby defective Au nanocrystal with an irregular shape, as quantified in Fig. 4(e). We suggest that the  $\{111\}$  facets of triangular Au islands may have a lower sticking and dissociation probability for digermene molecules than irregular surfaces and edges, as is known from other catalytic reactions.<sup>35</sup> From the growth rate, digermene pressure and dimensions of each Au island in Fig. 4(a), we calculate (see Sec. VI) a digermene sticking and incorporation probability of  $\sim 1\%$  on the triangles and 8% on the irregular island. The growth rates in the irregularly shaped Au nanocrystals are not dramatically different from measurements made during vertical nanowire growth from solid Au<sup>33</sup> and lateral growth in solid Au on amorphous substrates,<sup>32</sup> once we account for pressure and temperature. We conclude that the rate of growth front advance depends on the geometry of the system (collection area of Au crystal compared to area of the Au/Ge interface) as well as the nature of the Au surfaces.

As the Ge crystal grows, it remains fixed with respect to the substrate, while the Au increasingly becomes deformed and displaced [Fig. 4(b) and Movie M2], moving from its original site and eventually becoming more rounded [Fig. 2(a)]. Fluctuating strain fields associated with the deformation of the Au are visible during growth, and the Ge/Au interface advances in a jumpy fashion (Movie M2). Since Ge

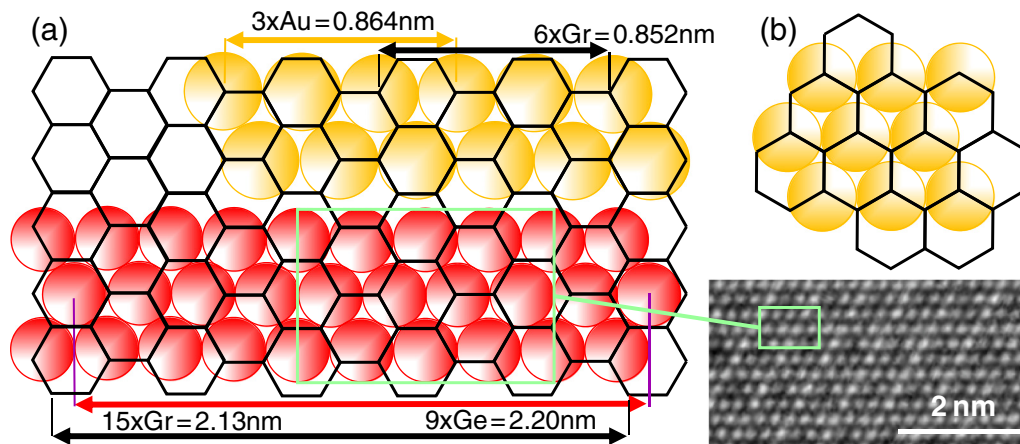


**FIG. 3.** Atomic structure of the Au/graphene and Ge/graphene interfaces. (a, b) Two possible arrangements, related by a 30° rotation, of a close packed layer of Au (yellow) placed on the honeycomb lattice of graphene. (a) Interface structure expected from the experimentally measured orientation relation between Au and graphene. It leads to a 0.86 nm supercell. Also shown is the interface structure of a close-packed layer of Ge (red) on graphene expected from the experimentally measured orientation relation. The structure is consistent with diffraction and with high resolution post-growth images of Ge on graphene (inset). (b) Structure with higher mismatch, not consistent with the experimental diffraction pattern.

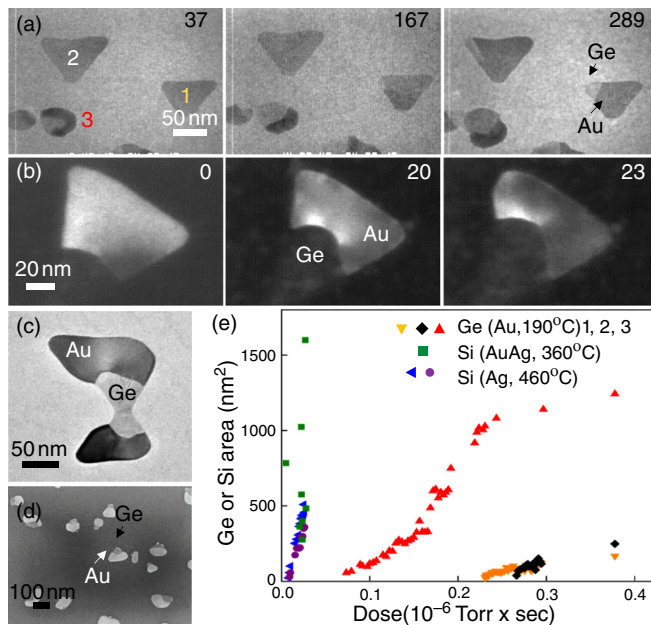


**FIG. 4.** Growth kinetics measurements. (a) Bright field images recorded during Ge growth at 190 °C and  $1.5 \times 10^{-5}$  Torr digermene on three-layer graphene after times indicated in minutes. (b) Dark field images recorded under the same conditions at the relative times indicated, showing strain fields, displacement, and reshaping of Au. The full datasets of (a, b) are shown in Movies M1 and M2, respectively. (c, d) Post growth images showing nucleation sites of Ge in an irregular Au island in bright field TEM and over a larger field of view in SEM, respectively. (e) Area of Ge and Si vs digermene or disilane dose for the three nanocrystals in (a) and for two Si nanocrystals grown from polycrystalline Ag and several nanocrystals grown from epitaxial Au + Ag, in both cases at  $1.4 \times 10^{-5}$  Torr and at the temperatures indicated.

presumably arrives at the catalyst crystal at a steady rate, the varying rate at which solid Ge is created hints at the presence of a reservoir of Ge (i.e., some Ge is present within or on the Au<sup>36</sup>). These aspects of growth appear insensitive to the substrate since Au-catalyzed Ge on hBN shows similar morphology and kinetics.

In the sample shown in Fig. 1(c), ~80% of the Ge nanocrystals (32 of 40 measured) were aligned with the Au and graphene. We find that solid, epitaxial catalysts are necessary to achieve this degree of epitaxy. With no catalyst (i.e., pyrolytic deposition with digermene), as shown in Fig. S5(a), Ge grown on graphene is polycrystalline. Furthermore, with a liquid catalyst (i.e., VLS-type growth<sup>4</sup>), Fig. S5(b), Ge shows only weak alignment, consistent with prior results.<sup>37</sup> Both these cases used higher growth temperatures than in Fig. 1, although similar precursor pressures. For the no-catalyst case in Fig. S5(a), sticking and dissociation directly on the substrate appeared very slow. Higher temperatures, above ~360 °C, were necessary to achieve a measurable Ge growth rate. For the liquid catalyst case in Fig. S5(b), a similar temperature was used. Growth from liquid catalysts first requires Ge and Au to react to form a eutectic melt. This might be expected to occur only above the Au-Ge eutectic temperature of 360 °C. However, liquid formation can take place below the eutectic temperature,<sup>33</sup> even as low<sup>32,34</sup> as 280 °C. Avoiding the formation of liquid guided the choice of temperature in Figs. 1 and 2. These comparisons between growth without catalyst, VLS growth from liquid

catalysts, and VSS growth from solid catalysts inform the process window to optimize Ge epitaxy on van der Waals substrates.

### III. EPITAXIAL SI ON VAN DER WAALS SUBSTRATES

The process outlined in Fig. 1 can be adapted to grow epitaxial Si. We first note that Si growth on graphene or hBN using disilane, either by direct CVD or from liquid catalytic droplets, produces only weak epitaxy [Figs. S5(c) and S5(d)]. This is similar to the case for Ge described above and again motivates the use of a solid, epitaxial catalyst and a VSS growth mode. However, disilane is chemically more stable than digermene and, compared to digermene, a higher temperature is needed to crack it efficiently.<sup>38</sup> In particular, cracking is extremely slow below the Au-Si eutectic temperature, so a VSS process using Au is not feasible. Instead, we need to choose a catalyst with an even higher eutectic temperature so that growth can take place below that temperature. A promising choice is Ag as it has a eutectic with Si<sup>39</sup> at 500 °C and has already been demonstrated as a catalyst for Si nanowire growth.<sup>40</sup> As deposited, Ag is in the form of islands that are not aligned with the substrate. The lack of in-plane texture can be seen from the circular diffraction rings in Fig. S6. Within individual grains, planar boundaries are visible, which may be twin boundaries or stacking faults. The observation of Ag islands being less well oriented and faceted compared to Au is consistent with other studies.<sup>17</sup> The results of VSS growth of Si on such Ag islands is shown in Figs. 5(a)–5(c). At 400 °C, Ag remains solid and Si does indeed nucleate from it. However, because the Ag is not oriented on the substrate, the Si crystal that forms is also not aligned with the substrate [Figs. 5(b) and 5(c)].

In order to improve the alignment of the Ag catalysts, we adopt a strategy of transferring the epitaxy from the substrate to Ag via Au.

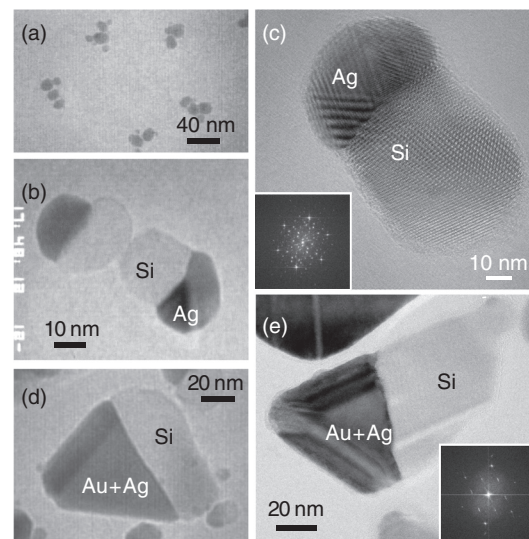


**FIG. 5.** Si growth from Ag and Au + Ag catalysts. (a) 2 nm Ag deposited on graphene showing irregular nanocrystals. (b) Image recorded during Si growth on Ag on graphene at 400 °C. The contrast in Ag indicates the presence of a planar boundary which may be a twin boundary or stacking fault. (c) High resolution image recorded after growth of Si from Ag on hBN; note planar defects in Ag and rotated Si lattice as seen in the inset FFT. (d) Image recorded during Si growth on Au + Ag on graphene at 360 °C and  $1.4 \times 10^{-5}$  Torr disilane. (e) Post-growth image of a large Si crystal with Si orientation shown in the inset FFT.

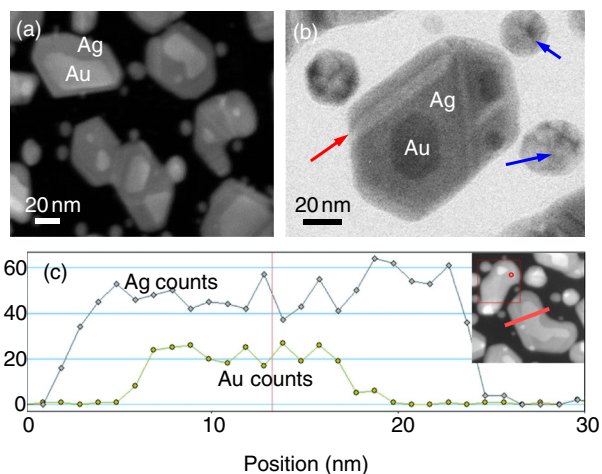


**FIG. 6.** Compositional analysis of AuAg nanocrystals on trilayer graphene. (a) HAADF STEM image after sequential deposition of 0.1 nm Au + 0.1 nm Ag on graphene. Au appears as bright triangles surrounded by darker Ag. (b) TEM image showing planar defects within Ag (red arrow) at the locations where the Ag around each Au island coalesces, implying the same orientation for the Ag around each Au island. Note the greater defect density in the Ag islands (blue arrows) that nucleated away from Au islands. (c) EDX scan along the line shown in the inset STEM image. The relatively constant Ag signal suggests uniform Ag thickness above and beside the Au.

In Fig. 6(a), we show that sequential deposition of Au followed by Ag produces composite islands that maintain the single crystal nature (both Au and Ag having the same structure and lattice parameter) and epitaxial quality of the Au. Energy dispersive x-ray analysis shows that Ag is deposited around and over the Au islands, Fig. 6. Note that some polycrystalline Ag forms between Au islands, so there is room for further optimization. The Au + Ag composite islands act as catalysts for Si deposition, Fig. 5(e), remaining solid during growth. The use of Au + Ag improves Si epitaxy with respect to growth using pure Ag, as can be seen by comparing Figs. 5(c) and 5(e). Furthermore, the use of Au + Ag also increases the reaction rate: measurements of growth rate from videos recorded during growth shows that Ag requires a higher temperature than Au + Ag to yield the same Si growth rate [Fig. 4(e)].

To summarize Figs. 1–6, Ge and Si nanocrystals can be grown epitaxially on graphene and hBN with the assistance of a catalyst. The highest level of epitaxy is achieved when the catalyst is a solid that is itself epitaxial with the substrate and transfers its alignment to the semiconductor. With no catalyst, or with a liquid catalyst, it appears that Si or Ge nuclei interact too weakly with the 2D substrate to result in a high degree of epitaxy. Although the requirement for a solid, epitaxial catalyst constrains the materials choices, we have shown that it is possible to transfer epitaxy through a chain of materials, using one metal (Au) that has robust epitaxial alignment to transfer its alignment to a second (Ag) that would otherwise lack good epitaxy. It would be interesting to evaluate similar transfer for other combinations of metals that form heterostructures with a well-defined orientation relationship.

#### IV. EXTENSION TO OTHER MATERIALS SYSTEMS

It is worthwhile to consider whether transferred epitaxy can be extended to other materials systems or more complex situations in

which epitaxial or patterned growth on van der Waals substrates would be useful. We first note that other van der Waals substrates may permit epitaxy of Si and Ge, provided that the substrate is stable under the growth conditions and that Au can be deposited epitaxially. Epitaxial Au has been reported on several van der Waals substrates including MoS<sub>2</sub>.<sup>17–19,21</sup> Layered minerals would be another interesting possibility since the epitaxy of Au on mica is well known, but growth of single crystal group IV semiconductors is a challenge.<sup>41</sup>

A second opportunity arises from the serial nature of the catalytic growth mode: modulation of the source gas could generate heterostructures (such as Si/Ge) or alloys, as has been demonstrated for nanowire growth with solid catalysts.<sup>42</sup> Indeed, based on the results in Figs. 1 and 5, many of the opportunities previously shown for catalytic nanowire growth, such as sharp heterostructures with VSS<sup>42</sup> or core-shell type structures,<sup>2</sup> can be considered for van der Waals substrates with interesting epitaxial possibilities. Since the catalyst position determines the growth location, patterning the catalyst (using the sensitivity of metal nucleation to defects on graphene, as in Fig. S3) could enable arrays of semiconductor nanostructures. Finally, a disadvantage of VSS is its slow growth rate. Faster growth could be achieved by establishing an epitaxial region of semiconductor and then raising the temperature to transition to a VLS growth mode.

Epitaxy on van der Waals substrates of semiconductors other than Si or Ge, such as GaAs, is an important objective for materials integration and for devices such as solar cells or diodes. We evaluated the morphology of GaAs on van der Waals substrates to test strategies based on catalytic growth. Figure 7 shows that exposure of graphene to trimethylgallium followed by arsine creates Ga droplets from which GaAs nucleates as hexagonal prisms and grows, with some suggestion of epitaxy, by motion of the droplet. GaAs nucleation is expected based on prior studies showing growth of GaAs<sup>43</sup> and GaN<sup>44</sup> on conventional substrates from Ga or AuGa liquid droplets. Epitaxy might be anticipated based on prior demonstrations of well-aligned vertical III–V nanowires grown on van der Waals substrates from Ga or AuGa

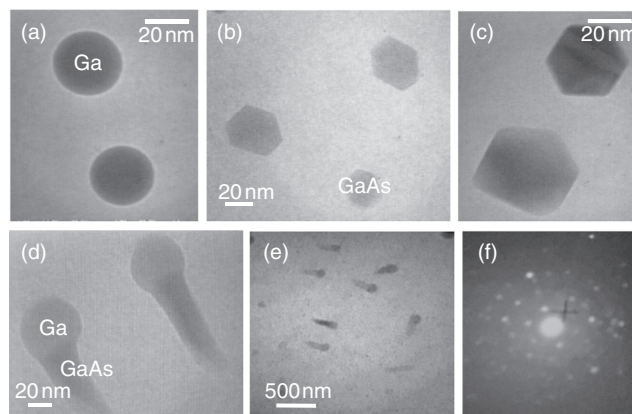


**FIG. 7.** GaAs droplet epitaxy on graphene. (a) Ga droplets formed by flowing trimethylgallium at 400 °C over graphene. (b, c) GaAs nuclei formed by flowing AsH<sub>3</sub> at  $1.5 \times 10^{-5}$  Torr and 400 °C over pre-formed Ga droplets. The nuclei become visible within a few seconds. The hexagonal shape suggests (0001) out of plane texture. (d, e) Lateral growth of GaAs nanowires imaged during flow of TMGa ( $5 \times 10^{-7}$  Torr) and arsine ( $1.5 \times 10^{-5}$  Torr) over Ga droplets. (f) Diffraction pattern from the area shown in (d) suggesting some alignment of the GaAs.

droplets.<sup>25,26</sup> However, under our growth conditions the GaAs extends laterally across the substrate to create semiconductor structures with dimensions similar to those in Figs. 2 and 5(c). We suggest that the epitaxy of these catalytically grown lateral nanostructures may be improved even further by the use of a solid catalyst such as Ag for GaAs.<sup>45</sup> This type of growth provides an alternative to the process of remote epitaxy,<sup>24</sup> in which single crystal III–V semiconductor thin films are templated on a 2D layer via a crystalline substrate beneath. The remote epitaxy mechanism is not applicable for suspended layers of 2D materials or for 2D layers on non-crystalline substrates. In such situations, a catalytic growth strategy may provide a pathway to epitaxy.

## V. CONCLUSIONS

We have demonstrated transferred epitaxy of important standard 3D semiconductors onto van der Waals-bonded substrates via catalytic deposition from gaseous precursors. Both liquid and solid phase catalysts permit semiconductor growth. Under the conditions we have examined for Si and Ge, the liquid phase catalysts composed of metal/semiconductor eutectic droplets (such as AuSi) generally do not improve the epitaxy of the deposited semiconductor compared to pyrolytic CVD. Instead, solid catalysts greatly improve the epitaxy, even at lower temperatures. The key requirement is to ensure that the solid catalyst nanocrystals are themselves aligned with the substrate to a higher degree than the semiconductor alone.

We believe that a general strategy that enables growth of 3D semiconductor nanocrystals epitaxially on van der Waals materials may impact device development and open new prospects for large-area deposition of functional nanostructures via low-cost substrates with transferred 2D layers.<sup>46</sup> The direct growth of 3D metal and semiconductor nanostructures on van der Waals substrates, in particular 2D materials, can expand the horizons for electronic and photonic applications and novel devices such as nanoantennas or single photon emitters that involve nanostructures of specific composition and geometry. Aligned arrays of semiconductor nanostructures on such substrates could enable designs for large area devices such as photovoltaics,<sup>13,15</sup> using technologies to grow or transfer 2D materials onto arbitrary substrates such as oxidized Si<sup>42</sup> to provide wafer-scale single crystal layers on inexpensive substrates. Nanostructures could be integrated with other materials that can already be grown onto van der Waals-bonded surfaces, such as covalent organic frameworks.<sup>47</sup> The use of a 2D material as the substrate also provides new options for device design, since the 2D material could be a free-standing layer, a flexible carrier layer, a diffusion barrier, part of the substrate of a flexible device,<sup>48</sup> or act as a stamp to transfer nanostructures onto other functionalized substrates.

Furthermore, epitaxy of semiconductors on 2D materials over a broader range of conditions, particularly at low temperatures, could open possibilities for substrates composed of flexible polymers or other temperature-sensitive materials. The low temperature semiconductor growth we have demonstrated, such as Ge below 200 °C, suggests increased possibilities for substrate materials that cannot tolerate higher temperatures.

We finally note that the directly observable growth with transmission electron microscopy through 2D substrates provides intriguing opportunities for evaluating the catalytic performance of individual particles as a function of their shape or defect structure. We

suggest that the use of metal nanoparticle catalysts provides an interesting approach to create and explore interfaces between 3D semiconductors and van der Waals-bonded materials, and forms a strategy that may be applicable to more complex and diverse materials systems.

## VI. METHODS

### A. Substrate preparation

Two types of custom fabricated substrates were used. One is a silicon nitride (SiN) chip patterned with a heater strip that enables temperature control and measurement [Fig. S1(a)]. Slots are patterned into the SiN between parts of the heater coil. These substrates were used for the data in Figs. S2(c), S2(e), S2(j) and S5. The other substrate, used for the majority of experiments, consists of a SiN membrane supported on Si, with 9 holes each 4 μm in diameter separated by 6 μm [Fig. S1(b)]. Graphene flakes were exfoliated from bulk natural graphite flakes (NGS Naturgraphit GmbH) on oxygen plasma treated Si/90 nm SiO<sub>2</sub> substrates. Flakes of suitable thickness were identified by their contrast in optical microscopy<sup>49</sup> and transferred using hydrophobic polymer cellulose acetate butyrate (CAB) as a handle.<sup>28,50</sup> Trilayer thickness was found to provide sufficient robustness for the *in situ* heating and growth experiments. Adding water to the SiO<sub>2</sub>/CAB interface detached the CAB with graphene attached to the polymer. The CAB with graphene flake was then transferred manually to the TEM sample carrier to cover multiple holes. Subsequently, the CAB was dissolved in acetone and rinsed in isopropyl alcohol before critical point drying. A similar process was used for hBN flakes, but here a thickness of 10 nm was chosen to enable strong moiré contrast for assessment of crystallographic relationships. The hBN was exfoliated from bulk hBN crystals from HQ Graphene. The samples were loaded into the UHV TEM vacuum chamber and annealed at 450 °C for at least four hours to remove polymer residues remaining from the transfer process. This combination of polymer and heat treatment is known to be effective in removing carbon and polymeric contamination;<sup>28,29</sup> material transferred using other polymers such as PMMA cannot be cleaned as effectively.<sup>51</sup>

### B. Metal deposition

Au and Ag were deposited with thicknesses between 0.2 and 2 nm from separate homebuilt K-cells using wire or sheet metal placed in a BN crucible. The K-cells are located within the vacuum system of the microscope but in a side chamber, so imaging is only possible after deposition. The deposited thickness was calibrated by measuring the evaporation rate immediately before and after deposition using a quartz crystal monitor. There is no intentional heating during metal deposition, but thermocouple measurements suggest that the sample temperature rises to 50–60 °C.

### C. Imaging

The samples were imaged using bright or dark field conditions in a Hitachi H-9000 TEM operated at 300 kV. Samples could be transferred between the evaporation chamber, annealing chamber, and TEM without breaking the vacuum. The samples were not imaged before metal deposition since irradiation alters nucleation, as shown in Fig. S2(d). Furthermore, when the metal deposition was characterized, only one part of the sample was imaged to avoid beam damage of the



2D material that may affect the semiconductor growth. For the  $\sim 40$  samples examined, triangles formed if the sample was annealed as described above. The presence of polymer residues or defects such as surface steps reduce the degree of epitaxy, Fig. S2, consistent with prior observations of Au deposition on graphite.<sup>52</sup>

#### D. Indexing diffraction patterns

The exact value of the camera length was determined by imaging regions of the 2D suspended material before metals or semiconductors were deposited. The additional  $d$  spacings (spots or rings) that appeared after deposition were then readily calculated and matched with the bulk structure of the deposited materials, allowing the epitaxial relationship between substrate and nanocrystal to be determined. The additional  $d$  spacings matched well with the expected values. However, it is important to note that unexpected spots are generally visible after Au deposition, as indicated in Figs. 1(a) and S3. From their relationship with the bulk Au reflections, we index these as Au  $1/3\{422\}$  at 0.250 nm. This reflection is “forbidden” on structure factor grounds but can be observed in thin crystals of the type analyzed here. When defects (dislocations, stacking faults) are not present, the intensity in the reflection is explained through shape effects (projection of higher order Laue zones) and surface steps (i.e., situations where the crystal is not an integral number of unit cells in thickness).<sup>53,54</sup>

#### E. Semiconductor deposition

For Ge and Si, digermane and disilane were used as precursors,<sup>55</sup> flowing the gases through a capillary tube with the pressure monitored by an ion gauge. The gas flow impinges on the top surface of the sample and the lower surface receives  $\sim 10\times$  less flux. For GaAs, we first flowed TMGa over a heated sample to form Ga droplets, then switched off TMGa and flowed AsH<sub>3</sub>, at which time GaAs nucleated rapidly. Alternatively, continuing flow of TMGa with the AsH<sub>3</sub> allowed sustained growth of Ga-catalyzed GaAs that formed lateral structures. Temperature calibration was achieved using an infrared pyrometer.

#### F. Post-growth characterization

Post-growth characterization was performed using TEM, SEM, and AFM. SEM imaging [Fig. 4(d)] was carried out using a Zeiss Leo III. AFM (Fig. S2) was carried out on a Veeco Digital Dimension-3100 (Bruker). High resolution TEM was carried out in a JEOL 2010F operated at 200 keV [Figs. 1(c), 1(e), 2(a), 5(c), and 5(e)] or the FEI Titan ETEM at Brookhaven National Laboratory operated at 80 keV (Figs. 4(c) and S5). HAADF STEM and EDX (Fig. 6) was carried out using a JEOL 3000 operated at 300 keV with an Emispec EDX system. The post-growth imaging was particularly important because the UHV TEM is not aberration corrected and does not have analytical capabilities. All imaging was carried out as soon as practical after removal of the sample from the UHV system. After several hours in air, oxide layers became visible around the Si, Ge, and even the metal. Ge is particularly sensitive to atmospheric exposure, and a few days of exposure causes complete conversion to amorphous oxide.

#### G. Moiré contrast analysis

The spacing and angle of the moiré patterns in Au and Ge [Figs. 1(b) and 2(a)] were measured with respect to the substrate lattice. These measurements were then compared with all possible moiré periods and angles for face centered and diamond cubic epilayers on a hexagonal substrate, for all relative rotations of the lattices, and including the possibility of up to  $\pm 1.25\%$  strain in the epilayer. The calculations used a geometric convolution technique<sup>55</sup> that considers every strong reflection, including structure factors, while also allowing for reflections such as Au  $1/3\{422\}$  that were observed experimentally, as discussed above. The comparison of calculated and experimental diffraction patterns shows in each case that zero strain and a specific rotation angle is consistent with the data.

#### H. Growth kinetics analysis

Values for sticking probability were calculated by assuming that the gas impinges at a rate  $J = N_A P. (2\pi MRT)^{-1/2}$ , or  $\sim 3$  monolayer/sec at  $10^{-5}$  Torr; that the impingement takes place over the top triangular facet of the nanocrystal; and that the Ge is the same height as the Au, assumed to be  $0.1\times$  the Au diameter. Ge and Si nanocrystal areas in Fig. 4(e) were obtained by measuring length and width.

#### SUPPLEMENTARY MATERIAL

The supplementary material includes captions for Movies M1 and M2, supporting Figs. S1–S6, and Movies M1 and M2.

#### AUTHOR CONTRIBUTIONS

The manuscript was written through contributions of all authors. P.P. performed UHV-TEM experiments and data analysis, J.D.T. and T.J.B. prepared samples, M.C.R. developed the UHV-TEM technique, D.Z. performed ETEM experiments, L.G. performed STEM imaging and EDX analysis, K.R. and G.V. performed moiré analysis, and S.H. and F.M.R. designed the experiments. All authors have approved the manuscript.

#### ACKNOWLEDGMENTS

This work was supported by the EPSRC (Grant Nos. EP/K016636/1 and EP/P005152/1) and ERC (Grant No. 279342: InSituNANO) (P.P., S.H.), the Danish National Research Foundation Center for Nanostructured Graphene (Project No. DNRF103) (J.D.T., T.B.) and the Lord Foundation of Massachusetts and an MIT MathWorks Engineering Fellowship (K.R.). This research used resources of the Center for Functional Nanomaterials, which is a U.S. DOE Office of Science Facility, at Brookhaven National Laboratory under Contract No. DE-SC0012704. The authors acknowledge Arthur W. Ellis for technical support.

#### DATA AVAILABILITY STATEMENT

The data that supports the findings of this study are available within the article and its supplementary material.

#### REFERENCES

- <sup>1</sup>A. Koma, “Van der Waals epitaxy for highly lattice-mismatched systems,” *J. Cryst. Growth* **201–202**, 236–241 (1999).

- <sup>2</sup>K. S. Novoselov, A. Mishchenko, A. Carvalho, and A. H. Castro Neto, "2D materials and van der Waals heterostructures," *Science* **353**, aac9439 (2016).
- <sup>3</sup>J. H. Lee, E. K. Lee, W.-J. Joo, Y. Jang, B.-S. Kim, J. Y. Lim, S.-H. Choi, S. J. Ahn, J. R. Ahn, M.-H. Park, C.-W. Yang, B. L. Choi, S.-W. Hwang, and D. Whang, "Wafer-scale growth of single-crystal monolayer graphene on reusable hydrogen-terminated germanium," *Science* **344**, 286–289 (2014).
- <sup>4</sup>N. P. Dasgupta, J. Sun, C. Liu, S. Brittman, S. C. Andrews, J. Lim, H. Gao, R. Yan, and P. Yang, "Semiconductor nanowires: Synthesis, characterization, and applications," *Adv. Mater.* **26**, 2137–2184 (2014).
- <sup>5</sup>A. P. Alivisatos, "Semiconductor clusters, nanocrystals, and quantum dots," *Science* **271**, 933–937 (1996).
- <sup>6</sup>Y. Xu, C. Cheng, S. Du, J. Yang, B. Yu, J. Luo, W. Yin, E. Li, S. Dong, P. Ye, and X. Duan, "Contacts between two- and three-dimensional materials: Ohmic, Schottky, and *p-n* heterojunctions," *ACS Nano* **10**, 4895–4919 (2016).
- <sup>7</sup>Y. Wang, J. C. Kim, R. J. Wu, J. Martinez, X. Song, J. Yang, F. Zhao, A. Mkhoyan, H. Y. Jeong, and M. Chhowalla, "Van der Waals contacts between three-dimensional metals and two-dimensional semiconductors," *Nature* **568**, 70–74 (2019).
- <sup>8</sup>S.-H. Bae, H. Kum, W. Kong, Y. Kim, C. Choi, B. Lee, P. Lin, Y. Park, and J. Kim, "Integration of bulk materials with two-dimensional materials for physical coupling and applications," *Nat. Mater.* **18**, 550–560 (2019).
- <sup>9</sup>D. Flötotto, Y. Ota, Y. Bai, C. Zhang, K. Okazaki, A. Tsuzuki, T. Hashimoto, J. N. Eckstein, S. Shin, and T.-C. Chiang, "Superconducting pairing of topological surface states in bismuth selenide films on niobium," *Sci. Adv.* **4**, eaar7214 (2018).
- <sup>10</sup>A. Allain, J. Kang, K. Banerjee, and A. Kis, "Electrical contacts to two-dimensional semiconductors," *Nat. Mater.* **14**, 1195–1205 (2015).
- <sup>11</sup>F. Xia, V. Perebeinos, Y.-M. Lin, Y. Wu, and P. Avouris, "The origins and limits of metal-graphene junction resistance," *Nat. Nanotechnol.* **6**, 179–184 (2011).
- <sup>12</sup>Y. Zhu, Y. Li, G. Arefe, R. A. Burke, C. Tan, Y. Hao, X. Liu, X. Liu, W. J. Yoo, M. Dubey, Q. Lin, and J. C. Hone, "Monolayer molybdenum disulfide transistors with single-atom-thick gates," *Nano Lett.* **18**, 3807–3813 (2018).
- <sup>13</sup>X. An, F. Liu, Y. J. Jung, and S. Kar, "Tunable graphene-silicon heterojunctions for ultrasensitive photodetection," *Nano Lett.* **13**, 909–916 (2013).
- <sup>14</sup>Y. Liu, J. Guo, L. Liao, S.-J. Lee, M. Ding, I. Shakir, V. Gambin, Y. Huang, and X. Duan, "Approaching the Schottky-Mott limit in van der Waals metal-semiconductor junctions," *Nature* **557**, 696–700 (2018).
- <sup>15</sup>L.-H. Zeng, M.-Z. Wang, H. Hu, B. Nie, Y.-Q. Yu, C.-Y. Wu, L. Wang, J.-G. Hu, C. Xie, F.-X. Liang, and L.-B. Luo, "Monolayer graphene/germanium Schottky junction as high-performance self-driven infrared light detector," *ACS Appl. Mater. Interfaces* **5**, 9362–9366 (2013).
- <sup>16</sup>Y. An, A. Behnam, E. Pop, and A. Ural, "Metal-semiconductor-metal photodetectors based on graphene/*p*-type silicon Schottky junctions," *Appl. Phys. Lett.* **102**, 013110 (2013).
- <sup>17</sup>D. W. Pashley, M. J. Stowell, M. H. Jacobs, and T. J. Law, "The growth and structure of gold and silver deposits formed by evaporation inside an electron microscope," *Philos. Mag.* **10**, 127–158 (1964).
- <sup>18</sup>K. Takayanagi, K. Yagi, K. Kobayashi, and G. Honjo, "Techniques for routine UHV *in situ* electron microscopy of growth processes of epitaxial thin films," *J. Phys. E: Sci. Instrum.* **11**, 441–448 (1978).
- <sup>19</sup>Y. Sun, H. Zhao, D. Zhou, Y. Zhu, H. Ye, Y. Aung Moe, and R. Wang, "Direct observation of epitaxial alignment of Au on MoS<sub>2</sub> at atomic resolution," *Nano Res.* **12**, 947 (2019).
- <sup>20</sup>A. C. Domask, K. A. Cooley, B. Kabius, M. Abraham, and S. E. Mohny, "Room temperature van der Waals epitaxy of metal thin films on molybdenum disulfide," *Cryst. Growth Des.* **18**, 3494–3501 (2018).
- <sup>21</sup>X. Liu, C.-Z. Wang, M. Hupalo, H.-Q. Lin, K.-M. Ho, and M. C. Tringides, "Metals on graphene: interactions, growth morphology, and thermal stability," *Crystals* **3**, 79–111 (2013).
- <sup>22</sup>R. Monna, D. Angermeier, A. Slaoui, and J. C. Muller, "Polycrystalline silicon thin films by rapid thermal chemical vapor deposition (RTCVD) on graphitic surfaces," *Proceedings of the Conference Record of the IEEE Photovoltaic Specialists Conference, Washington, DC, May 13–17, 1996 (IEEE, Piscataway, NJ, 2002)*, 701–704.
- <sup>23</sup>W. Xiao, Z. Yan, S. S. Kushvaha, M. Xu, and X. S. Wang, "Different growth behavior of Ge, Al and Sb on Graphite," *Surf. Rev. Lett.* **13**, 287–296 (2006).
- <sup>24</sup>Y. Kim, S. S. Cruz, K. Lee, B. O. Alawode, C. Choi, Y. Song, J. M. Johnson, C. Heidelberger, W. Kong, S. Choi, K. Qiao, I. Almansouri, E. A. Fitzgerald, J. Kong, A. M. Kolpak, J. Hwang, and J. Kim, "Remote epitaxy through graphene enables two-dimensional material-based layer transfer," *Nature* **544**, 340–343 (2017).
- <sup>25</sup>A. M. Munshi, D. L. Dheeraj, V. T. Fauske, D. C. Kim, A. T. van Helvoort, B. O. Finland, and H. Weman, "Vertically aligned GaAs nanowires on graphite and few-layer graphene: Generic model and epitaxial growth," *Nano Lett.* **12**, 4570–4576 (2012).
- <sup>26</sup>P. K. Mohseni, A. Behnam, J. D. Wood, C. D. English, J. W. Lyding, E. Pop, and X. Li, "In<sub>x</sub>Ga<sub>1-x</sub>As nanowire growth on graphene: Van der Waals epitaxy induced phase segregation," *Nano Lett.* **13**, 1153–1161 (2013).
- <sup>27</sup>J. D. Thomsen, T. Gunst, S. S. Gregersen, L. Gammelgaard, B. S. Jessen, D. M. A. Mackenzie, K. Watanabe, T. Taniguchi, P. Bøggild, and T. J. Booth, "Suppression of intrinsic roughness in encapsulated graphene," *Phys. Rev. B* **96**, 014101 (2017).
- <sup>28</sup>J. D. Thomsen, J. Kling, D. M. A. Mackenzie, P. Bøggild, and T. J. Booth, "Oxidation of suspended graphene: Dynamics and stability beyond 1000 °C," *ACS Nano* **13**(2), 2281–2288 (2019).
- <sup>29</sup>E. L. Evans, O. P. Bahl, and J. M. Thomas, "The decoration of and epitaxial growth of gold on graphite surfaces," *Carbon* **5**, 587–588 (1967).
- <sup>30</sup>T. P. Darby and C. P. Wayman, "The growth of Au films on graphite in ultra high vacuum," *Phys. Status Solidi (a)* **1**, 729–748 (1970).
- <sup>31</sup>B. J. Kim, C.-Y. Wen, J. Tersoff, M. C. Reuter, E. A. Stach, and F. M. Ross, "Growth pathways in ultra-low temperature Ge nucleation from Au," *Nano Lett.* **12**, 5867–5872 (2012).
- <sup>32</sup>S. Kodambaka, J. Tersoff, M. C. Reuter, and F. M. Ross, "Germanium nanowire growth below the eutectic temperature," *Science* **316**, 729–732 (2007).
- <sup>33</sup>A. D. Gamalski, J. Tersoff, R. Sharma, C. Ducati, and S. Hofmann, "Formation of metastable liquid catalyst during subeutectic growth of germanium nanowires," *Nano Lett.* **10**, 2972–2976 (2010).
- <sup>34</sup>N. M. Andoy, X. Zhou, E. Choudhary, H. Shen, G. Liu, and P. Chen, "Single-molecule catalysis mapping quantifies site-specific activity and uncovers radial activity gradient on single 2D nanocrystals," *J. Am. Chem. Soc.* **135**, 1845–1852 (2013).
- <sup>35</sup>B. J. Kim, J. Tersoff, S. Kodambaka, M. C. Reuter, E. A. Stach, and F. M. Ross, "Kinetics of individual nucleation events observed in nanoscale vapor-liquid-solid growth," *Science* **322**, 1070–1073 (2008).
- <sup>36</sup>E. Mataev, S. K. Rastogi, A. Madhusudan, J. Bone, N. Lamprinakos, Y. Picard, and T. Cohen-Karni, "Synthesis of group IV nanowires on graphene: The case of Ge nanocrawlers," *Nano Lett.* **16**, 5267–5272 (2016).
- <sup>37</sup>K. Yoshida, K. Matsumoto, T. Oguchi, K. Tonokura, and M. Koshi, "Thermal decomposition of disilane," *J. Phys. Chem. A* **110**(14), 4726–4731 (2006).
- <sup>38</sup>R. W. Olesinski, A. B. Gokhale, and G. J. Abbaschian, "The Ag-Si (Silver-Silicon) system," *Bull. Alloy Phase Diagrams* **10**, 635–640 (1989).
- <sup>39</sup>J. V. Wittemann, W. Münchgesang, S. Senz, and V. Schmidt, "Silver catalyzed ultrathin silicon nanowires grown by low-temperature chemical-vapor-deposition," *J. Appl. Phys.* **107**, 096105 (2010).
- <sup>40</sup>A. J. Littlejohn, Y. Xiang, E. Rauch, T.-M. Lu, and G.-C. Wang, "Van der Waals epitaxy of Ge films on mica," *J. Appl. Phys.* **122**, 185305 (2017).
- <sup>41</sup>C.-Y. Wen, M. C. Reuter, J. Bruley, J. Tersoff, S. Kodambaka, E. A. Stach, and F. M. Ross, "Formation of compositionally abrupt axial heterojunctions in Si/Ge nanowires," *Science* **326**, 1247–1250 (2009).
- <sup>42</sup>S. Plissard, G. Larrieu, X. Wallart, and P. Caroff, "High yield of self-catalyzed GaAs nanowire arrays grown on silicon via gallium droplet positioning," *Nanotechnol.* **22**, 275602 (2011).
- <sup>43</sup>M. Gherasimova, G. Cui, S. R. Jeon, Z. Ren, D. Martos, and J. Han, "Droplet heteroepitaxy of GaN quantum dots by metal-organic chemical vapor deposition," *Appl. Phys. Lett.* **85**, 2346 (2004).
- <sup>44</sup>C. Lindberg, A. Whitticar, K. A. Dick, N. Sköld, J. Nygård, and J. Bolinsson, "Silver as seed-particle material for GaAs nanowires: Dictating crystal phase and growth direction by substrate orientation," *Nano Lett.* **16**, 2181–2188 (2016).
- <sup>45</sup>Y. Lee, S. Bae, H. Jang, S. Jang, S. E. Zhu, S. H. Sim, Y. Song, B. H. Hong, and J. H. Ahn, "Wafer scale synthesis and transfer of graphene films," *Nano Lett.* **10**, 490–493 (2010).

- <sup>46</sup>J. W. Colson, A. R. Woll, A. Mukherjee, M. P. Levendorf, E. L. Spitzer, V. B. Shields, M. G. Spencer, J. Park, and W. R. Dichtel, "Oriented 2D covalent organic framework thin films on single-layer graphene," *Science* **332**(6026), 228–231 (2011).
- <sup>47</sup>J. Kim, M. Kim, M.-S. Lee, K. Kim, S. Ji, Y.-T. Kim, J. Park, K. Na, K. H. Bae, H. K. Kim, F. Bien, C. Y. Lee, and J.-U. Park, "Wearable smart sensor systems integrated on soft contact lenses for wireless ocular diagnostics," *Nat. Comm.* **8**, 14997 (2017).
- <sup>48</sup>B. S. Jessen, P. R. Whelan, D. M. A. Mackenzie, B. Luo, J. D. Thomsen, L. Gammelgaard, T. J. Booth, and P. Boggild, "Quantitative optical mapping of two-dimensional materials," *Scientific Rep.* **8**, 6381 (2017).
- <sup>49</sup>G. F. Schneider, V. E. Calado, H. Zandbergen, L. M. K. Vandersypen, and C. Dekker, "Wedging transfer of nanostructures," *Nano Lett.* **10**, 1912–1916 (2010).
- <sup>50</sup>Y.-C. Lin, C.-C. Lu, C.-H. Yeh, C. Jin, K. Suenaga, and P.-W. Chiu, "Graphene annealing: How clean can it be?," *Nano Lett.* **12**, 414–419 (2012).
- <sup>51</sup>J. J. Metois, J. C. Heyraud, and Y. Takeda, "Experimental conditions to obtain clean graphite surfaces," *Thin Solid Films* **51**, 105 (1978).
- <sup>52</sup>D. Cherns, "Direct resolution of surface atomic steps by transmission electron microscopy," *Philos. Mag.* **30**, 549–556 (1974).
- <sup>53</sup>J. Reyes-Gasga, A. Gómez-Rodríguez, X. Gao, and M. José-Yacamán, "On the interpretation of the forbidden spots observed in the electron diffraction patterns of flat Au triangular nanoparticles," *Ultramicroscopy* **108**, 929–936 (2008).
- <sup>54</sup>F. M. Ross, "Controlling nanowire structures through real time growth studies," *Rep. Prog. Phys.* **73**, 114501 (2010).
- <sup>55</sup>P. Zeller and S. Günther, "What are the possible moiré patterns of graphene on hexagonally packed surfaces? Universal solution for hexagonal coincidence lattices, derived by a geometric construction," *New J. Phys* **16**, 083028 (2014).